Applications

Simulation

Simulation: Transactions of the Society for Modeling and Simulation International
1–11

DOI: 10.1177/0037549717705466
journals.sagepub.com/home/sim
SAGE SCS

Simulation of FPGA controlled Single Stage Boost Inverter for the Applications of Grid Connected Photovoltaic System

B. Meenakshi Sundaram[1], B.V. Manikandan[2] and M. Kaliamoorthy[3]

Abstract

Improving the efficiency, reducing the cost and maintaining the power quality of a grid tied with Photovoltaic (PV) system are the important aspects of the present day research. The efficiency of power conversion can be improved by reducing the number of stages. In this paper, a single stage boost inverter topology fed from PV array is used and connected to a single phase grid. Less number of switching components is used in this topology compared to conventional technique and hence, the converter losses are reduced. This can also be very well extended to utility grid system. Further, the proposed topology includes battery backup unit which consists of a DC-DC converter to overcome the variations of Voltage based Maximum Power Point (VMPP) of PV array because of the variations in solar irradiance. The proposed system uses the current control approach which has zero steady state tracking error to control the single stage boost inverter. The proposed system offers many advantages such as low cost, high efficiency, compactness and high quality of output power. Design procedure and simulation results are obtained from MATLAB/SIMULINK and the experimental results are obtained from the model developed in the laboratory. The entire system is controlled by SPATRAN 3A FPGA board.

Keywords

Boost Inverter, Photovoltaic, Grid Connected Inverter, Maximum Power Point, Current Control Strategy

1. Introduction

Presently, the growing energy demand for conventional sources like coal, natural gas and crude oil has driven the society towards the research and development of alternate energy sources. A lot of renewable sources like wind energy, solar or photovoltaic (PV) and Fuel cells are being widely used. These energy sources are preferred because they are ecological friendly. The Photovoltaic energy has become one of the most prominent sources of energy and due to this fact, the PV energy is free and sustainable.[1]

Due to the stochastic nature, the PV systems essentially require a power conditioning unit. But, the PV systems should have backup unit to ensure the reliable power at the load terminals.[2] Further, the PV systems also require an inversion stage, when they are connected to autonomous AC loads or to an electrical grid.[3] The output voltage and power of a low-power PV module are typically low and they vary with respect to the environmental conditions.[4] Several researchers have utilized a multistage PV fed power conditioning system to deliver power to ac loads.[5-11]

Compared to single stage power conversion systems, the multistage power conversion system possesses several disadvantages such as expensive, bulky and inefficient.[12] To overcome the above said drawbacks, a single stage power converter topology has been proposed and it is capable of inverting and boosting the DC input voltage simultaneously with reduced power switches.[13-14]

To enhance the performance of this single stage topology during the transient conditions, a double loop control strategy with voltage control is proposed.[15] In order to control the power fed into the grid, a current control

[1]Assoc. Professor/EEE, Sethu Institute of Technology, Kariapatti, Tamil nadu, India
[2]Professor/EEE, Mepco Schlenk Engineering College, Sivakasi, Tamil nadu, India
[3]Assoc. Professor/EEE, Dr.Mahalingam College of Engg. and Tech., Pollachi, Tamil nadu, India

Corresponding author:
B. Meenakshi Sundaram, Associate Professor / EEE, Sethu Institute of Technology, Kariapatti, Virudhunagar District, Tamilnadu 626115 India.
Email: bmsapk@gmail.com

strategy is also employed in the distributed grid-connected inverters.[16] Hence, the characteristics of operation and the performance of grid connected PV fed single stage current controlled boost inverter system are important breakthroughs which have not yet been reported in the technical literature. Further in this work, a Field Programmable Gate Array (FPGA) based control is used to control the developed inverter, which has higher speed, flexibility and integrated design tools compared to other modes of control.

The main objective of the paper is to realize a single-phase grid-connected current controlled PV system which has only one power conversion stage and it offers high power conversion efficiency, low cost and reduced converter size. The proposed scheme is experimentally executed and implemented using FPGA.

The paper has been organized as follows: The proposed grid-connected current controlled PV system along with the inverter topology, the backup energy storage unit and the current control algorithm is focused in Section II. Section III presents the simulation and the experimental results to validate the performance of the proposed PV system. Section IV depicts the summary of the conclusions.

2. System Configuration

The PV fed grid connected current controlled single stage boost inverter is presented in Figure 1. It consists of two boost converters which are connected to the same DC input and the backup bidirectional converter unit. The boost inverter is fed by the PV modules and also by the battery backup unit. The PV modules and the battery backup unit are connected to an irregular DC bus. But, the output of the boost inverter is connected to the local load and the grid through inductances (L_f and L_0). The system combines the output current control of boost converter 1 and the output voltage control of boost converter 2.

The first control objective is to obtain the output current i_{grid} in phase with grid voltage v_{grid}.

$$v_{grid} = V_{grid} \sin(\omega_0 t) \tag{1}$$

The reference output current i^*_{grid} is defined as

$$i^*_{grid} = I_{grid} \sin(\omega_0 t) \tag{2}$$

where I_{grid} depends on the output power of the inverter. The output current is described as

$$L_0 \frac{di_{grid}}{dt} = v_{b1} - v_{b2} - v_{grid} \tag{3}$$

where v_{b1} and v_{b2} are the output voltages of boost converters 1 and 2, respectively.

The difference between v_{b1} and v_{b2} controls the output current of the inverter and hence, there are many permutations of v_{b1} and v_{b2} to attain the current control. The second objective is to maintain balanced voltage and power in both the boost converters. As a result, the two identical

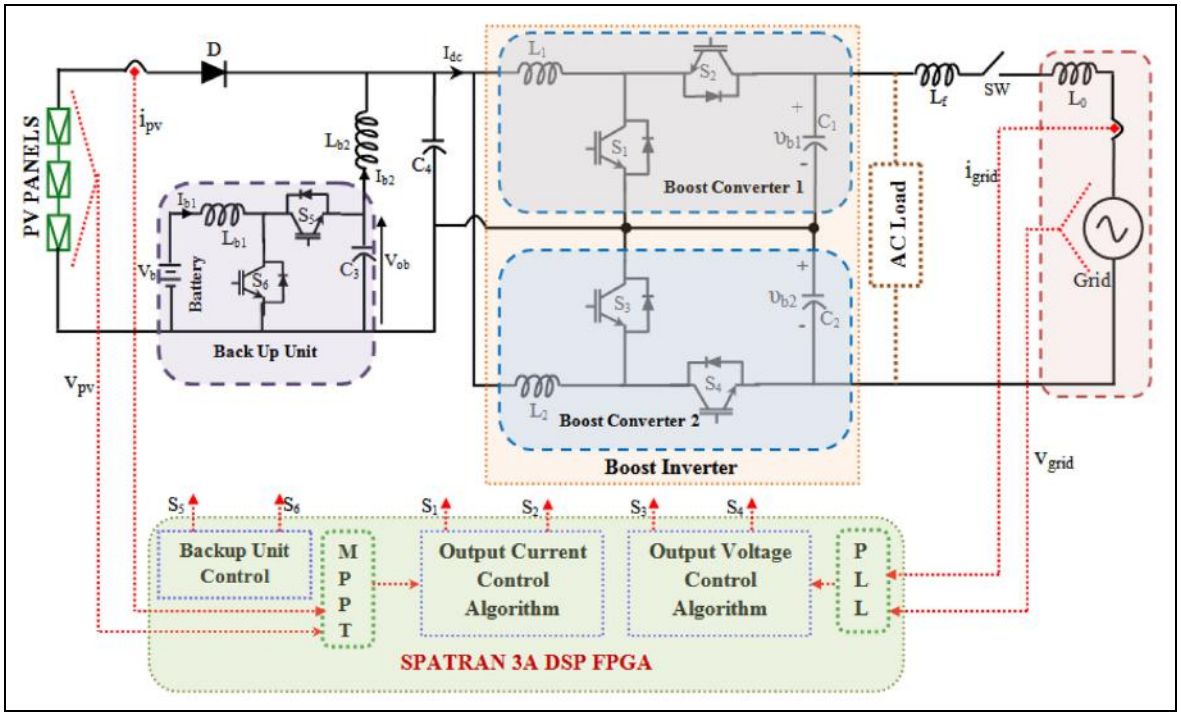

Figure 1. Proposed grid connected PV fed simultaneous voltage and current controlled single stage boost inverter.

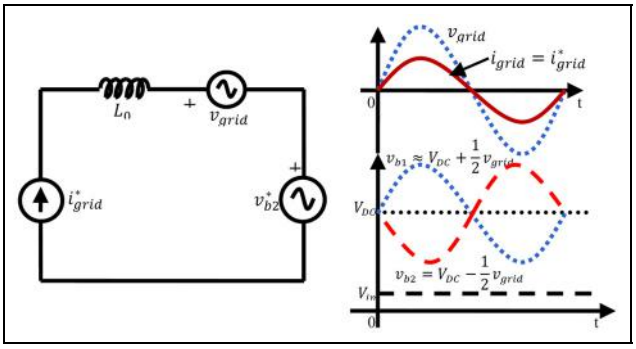

Figure 2. Equivalent circuit of grid connected PV system (a) Boost converter 1 and 2 controlled separately (b) Expected Controlled waveforms.

power stages can be utilized. From Figure 2, it can be seen that the boost converter 1 controls the current which follows the reference current i^*_{grid} and the boost converter 2 controls the voltage which follows the reference voltage v^*_{b2}. It is also provided as

$$v^*_{b2} = V_{DC} - \frac{1}{2}v_{grid}. \tag{4}$$

By neglecting the small voltage drop across L_0, the output voltage v_{b1} becomes

$$v^*_{b1} \approx V_{DC} + \frac{1}{2}v_{grid} \tag{5}$$

where V_{DC} is the bias DC voltage which guarantees that the values of sinusoidal v_{b1} and v_{b2} are greater than that of the input DC voltage V_{in}. Various researchers have dealt this concept.[12-17]

In the proposed work, the current and voltage controls are chosen for the boost converters 1 and 2, respectively, since this is the most suitable technique for controlling the individual boost converter by covering the wide operating points. The control has been designed based on the cascading control, feedback linearization and PR controllers. The control block diagram of boost inverter is shown in Figure 3.

2.1. Photovoltaic Array Model

The most widely used model for a PV cell is the single-diode equivalent circuit model.[14] The relationship between the PV cell output voltage (V) and the PV cell current (I) can be expressed as,

$$I = I_L - I_D = I_L - I_0\left[\exp\left(\frac{V + IR_s}{\propto}\right) - 1\right] \tag{6}$$

where I_L is the light generated current in amperes, I_0 is the reverse saturation current of the diode in amperes, I is the load current in amperes,V is the PV cell output voltage in volts, R_s is the series resistance in ohms and α is the thermal voltage timing completion factor which is also known as curve fitting parameter.

2.1.1. Determination of Light Current I_L

$$I_L = \frac{\phi}{\phi_{ref}}\left[I_{L,ref} + \mu_{I,SC}\left(T_C - T_{C,ref}\right)\right] \tag{7}$$

where ϕ is the irradiance of the geographical location (W/m^2). ϕ_{ref} is the reference irradiance given by the

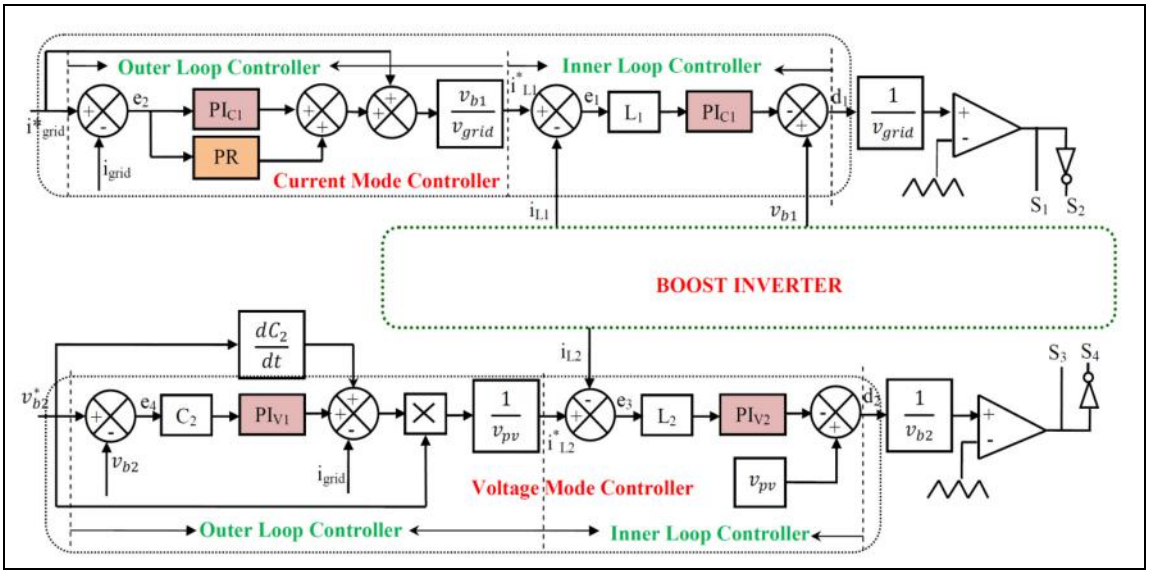

Figure 3. Control Block Diagram of Boost Inverter.

manufacturer obtained in Standard Testing Condition (STC i.e. 1000 $\frac{W}{m^2}$ is generally used). I_L, ref is the light current at the reference condition (also known as short circuit current, $I_{SC,ref}$) (i.e. 1000 $\frac{W}{m^2}$ and 25°C). T_c is the PV cell temperature in degree centigrade. $T_{c,ref}$ is the reference temperature under STC (25°C is generally used). $\mu_{I,SC}$ is the temperature coefficient of the short circuit current (A/°C). Both $I_{L,ref}$ and $\mu_{I,SC}$ will be provided by the manufacturer.

2.1.2. Determination of Saturation Current I_0.

$$I_0 = I_{0,ref} + \left(\frac{T_{c,ref} + 273}{Tc + 273}\right)^3 \exp\left[\frac{e_{gap}N_s}{q\alpha_{ref}}\left(1 - \frac{T_{c,ref} + 273}{Tc + 273}\right)\right] \quad (8)$$

Where $I_{0,ref}$ is the saturation current at the STC in amperes, e_{gap} is the band gap of the PV material (1.17eV for silicon materials),N_s is the number of cells in series in a PV module, q is the charge of an electron (1.6021773310-19 Coulombs) and α_{ref} is the value of alpha at reference condition.

2.1.3. Determination of Thermal Voltage Timing Completion Factor. In order to calculate the thermal voltage timing completion factor (Curve fitting factor), it is necessary to determine its value under STC.The value of α_{ref} is given by,

$$\propto_{ref} = \frac{2V_{mp,ref} - V_{oc,ref}}{\frac{I_{SC,ref}}{I_{SC,ref} - I_{mp,ref}} + \ln\left(1 - \frac{I_{mp,ref}}{I_{SC,ref}}\right)} \quad (9)$$

Where $V_{mp,ref}$ is the voltage of PV module at maximum power point under STC (V). $I_{mp,ref}$ is the current of PV module at maximum power point under STC (A). $I_{SC,ref}$ is the short circuit current of PV module at STC (A).The thermal voltage timing completion factor (α) is the function of temperature, which is expressed as,

$$\propto = \left(\frac{T_c + 273}{Tc, ref + 273}\right)\propto_{ref}. \quad (10)$$

2.1.4. Determination of Series Resistance, R_s. Some manufacturers of the PV module provide the value of Rs in their data sheet. If it is not provided, the value of Rs can be calculated using the following expression

$$R_s = \frac{\propto_{ref} \ln\left(1 - \frac{I_{mp,ref}}{I_{SC,ref}}\right) + V_{OC,ref} - V_{mp,ref}}{I_{mp,ref}}. \quad (11)$$

2.1.5. Thermal Model of PV cell. From the above expressions (6)-(11), it is very clear that the temperature plays a vital role in the PV module performance. Therefore, it is necessary to determine the thermal model of the PV module. A lumped thermal model proposed by (Oystein Ulleberg, 1998)[14] has been used in this present study. The temperature of the PV module is affected by its ambient temperature, irradiation, PV module voltage and current. The dynamic equation for cell temperature is expressed as,

$$C_{PV}\frac{dT_c}{dt} = k_{in,PV}\phi - \frac{VxI}{A} - k_{loss}(T_c - T_a) \quad (12)$$

Where C_{PV} is the thermal capacitance of the PV module [J/($°C.m^2$)],K_{in}, PV is the transmittance absorption product of the PV module, K_{loss} is the overall heat loss coefficient of the PV module [W/ ($°C.m^2$],T_a is the ambient temperature in degree centigrade and A is the effective area of the PV module in m^2.

2.2. Current Mode Control of Boost Converter 1

The current mode control diagram of boost converter 1 is shown in Fig. 3. From the left to the right, it comprises two parts: the outer-loop controller and the inner-loop controller. In this approach, the average switching model is employed in the Continuous Conduction Mode (CCM) is employed because, the boost converter operates on bidirectional way and it always works under the CCM. It should perfectly present the dynamic performance at the lower half of the switching frequency. Here,the inner loop is built to control the inductor current i_{L1}, which is from the outer loop, in order to track the reference i_{L1}*. With different frequency scales, these two control loops can be examined and designed separately. To derive proper controllers, Feedback linearization is utilized in each loop. To obtain better tracking performance, the Proportional Resonant controllers can be designed after the linearization.

2.3. Voltage Mode Control of Boost Converter 2

The voltage mode control diagram of boost converter 2 is shown in Fig. 3. This control structure also has two controllers namely the outer loop controller and the inner loop controller. The inner loop controller is used to control the inductor current i_{L2} and the outer loop controller is used to control the capacitor voltage v_{b2}. The reference current for the inner loop is obtained from the output of the outer loop (i.e. i_{L2}*). Similar to the current mode control design, the voltage mode controllers can also be designed separately in different frequency scales. The designs of both the voltage mode and the current mode controls are clearly described in [16].

2.4. Backup Unit Control

The backup unit control is essential for the boost inverter operation and it is divided into two parts. First, the backup unit is designed to maintain the slow dynamics of the PV. Secondly, it supplies low-frequency ac current to facilitate

Table 1. Modes of Operation of Backup Unit for Load Change

P_3 Increase	P_3 Decrease	Normal
$P_1 + P_2 \rightarrow P_3$	$P_1 \rightarrow P_2 + P_3$	$P_1 = P_3$
Discharge		
↓	Charge	
Charge	↓	Normal
↓	Normal	
Normal		
$P_1 \rightarrow$ Power Delivered from PV panel		
$P_2 \rightarrow$ Power Delivered from Back up unit		
$P_3 \rightarrow$ Power Delivered from by the inverter		

the protection of the PV system. The low-frequency current ripple of the batteries has an impact on their lifetime.[18] Generally, cheap battery components are preferred because they provide low-frequency current ripple. Moreover, the backup unit comprises a current-mode controlled bidirectional converter and a battery for energy storage. For example, when 1-kW load is connected to a no-load condition of the system, the backup unit immediately supplies 1-kW power from the battery to the load, as shown in Table 1.

Simultaneously, the surplus power from the PV could be recovered and stored in the battery, when the load is disconnected abruptly. This will increase the overall efficiency of the energy system.

The backup unit controller is proposed in this study to control the output current of the backup unit. It is shown in Fig. 4. The reference current of I_{Lb1} is determined by I_{dc} through a low-pass filter and the demanded current I_{demand} is correlated with the load change. The ac component of the current reference eliminates the ac ripple current in the PV power module whereas the dc component deals with the slow dynamics of the PV.

2.5. Current Based Maximum Power Point Tracking

For the given atmospheric conditions (mainly dependent on temperature[1] and insolation level), the photovoltaic (PV) cells supply the maximum power at a particular operating point ie.Maximum Power Point (MPP). Several different MPPT techniques have been proposed in the literature.[19-24] The techniques summarized in [25] can be classified as: (1) Look-up table methods, (2) Perturbation and observation methods, and (3) Model-based computational methods. There are two major techniques in the Model-based computational methods.They are Voltage-based MPPT (VMPPT) and Current-based MPPT (CMPPT) techniques. Masoum et al., have analyzed both CMPPT and VMPPT techniques for matching resistive loads and DC motor loads.[26] Whereas Enslin et al.,[27] have used CMPPT method for matching a DC motor load. In the present research work, CMPPT method is proposed to obtain maximum power for the PV array.

The primary idea behind the current-based MPPT is that the current at the maximum power point I_{mp} has a strong linear relationship with the short circuit current I_{sc}. I_{sc} can either be measured on line under different operation conditions or computed from a validated model. Figure 5 shows the curve of I_{mp} vs I_{sc} of Tata BP solar panel (TP180). The data points of I_{mp} vs I_{sc} are fitted using curve fitting tool box of MATLAB/SIMULINK. It can be noted that I_{mp} has a very good linear dependence on I_{sc} and it can be expressed as:

$$I_{mp} = k_{cmppt} x I_{sc} - C \tag{13}$$

where k_{cmppt} is the current factor of CMPPT control and ''C'' is a constant, which is dependent on the cell temperature. Once the value of I_{sc} is known, I_{mp} can be calculated easily from the above relation. The value of I_{mp}, which is i_{pv}, obtained from eqn (6) is given as set point reference i_{grid}^* . The parameters of TP180 are given in Table 2.

3. Simulation and Experimental Results

To validate the effectiveness and the performance, the proposed Photovoltaic based single stage boost inverter is simulated and it is also tested experimentally.The simulations are performed using MATLAB/SIMULINK

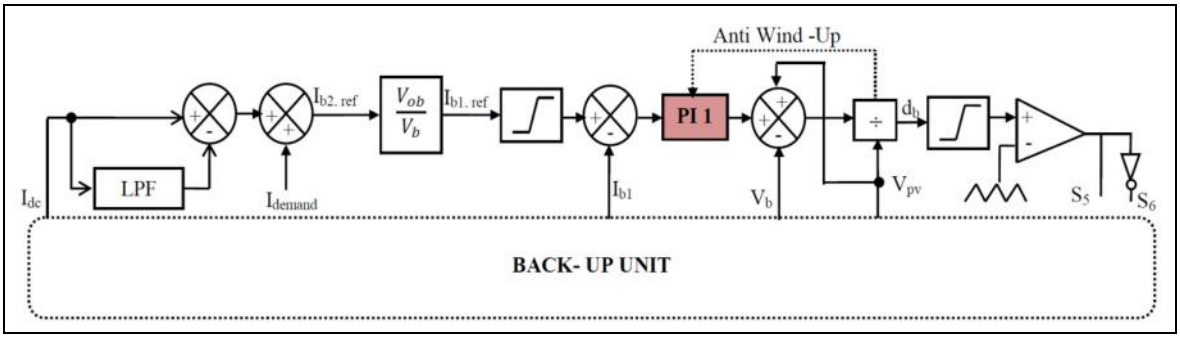

Figure 4. Control Block Diagram of Back-up unit.

Table 2. Parameters of TATA BP Solar PV Module (TP180)

Parameters	Values
Voltage at maximum power point($V_{mp,ref}$)	35.8 V
Current at maximum power point($I_{mp,ref}$)	5.03 A
Open circuit voltage at STC ($V_{OC,ref}$)	43.6 V
Short circuit current at STC ($I_{SC,ref} = I_{L,ref}$)	5.48 A
Reference Irradiance (φ_{ref})	1000 w/m^2
Reference cell temperature ($T_{c,ref}$)	25 °C
Thermal capacitance (C_{pv})	5 X 10^4 J/ (°C.m^2)
Area of the PV module (m^2)	1.25
Transmittance absorption product ($K_{in,PV}$)	0.9
Heat loss coefficient (K_{loss})	30 W/ (°C.m^2)
Temperature coefficient ($\mu_{I,SC}$)	0.038
Module Power at STC	180 Watts

Table 3. Simulation and Experimental Parameters

Parameters	Values
PV panel output voltage	31V-38 V (200 w/m^2 to 1200 w/m^2)
AC output voltage	220V, 50Hz
Switching Frequency	20KHz
Rated Power	1KW
Controller	SPATRAN 3A DSP
Voltage Sensor	LEM LV25-p
Current Sensor	LEM HAL50s
Energy Storage	12V-24Ah lead acid batteries (2Nos)
$L_1 = L_2$	120mH
$L_{b1} = L_{b2}$	150 μH
L_f	5mH
$C_1 = C_2 = C_3 = C_4$	30μF
PR	$\frac{0.015s}{s^2+98696}$
PI_{C1}	K_P = 0.175 and K_I = 1750
PI_{C2}	K_P = 18750 and K_I = 520875
PI_{V1}	K_P = 1909 and K_I = 190900
PI_{V2}	K_P = 18750 and K_I = 520875
Relative tolerance	1e-3
Maximum step size	1e-5
Minimum step size	1e-6
Solver	ODE23tb(stuff/TR-BDF2)
Zero Crossing Control	Local Settings

software. The AC output of the system is chosen as 220 V, 50 Hz whereas the DC input voltage is allowed to vary between 31 V and 38 V. The parameters used for simulation and experimentation are shown in Table 3.

The simulation diagram of the proposed Photovoltaic fed single stage boost inverter is shown in Figure 6. The proposed MPPT algorithm is simulated for step change in the irradiance level.Irradiance pattern used for testing the MPPT algorithm is shown in Figure 7 and its corresponding output obtained from the MPPT algorithm is shown in Figure 8. The output voltage of the boost inverter along with the capacitor voltages is illustrated in Figure 9. Figure 10 represents the grid voltage and grid current at Point of Common Coupling (PCC).

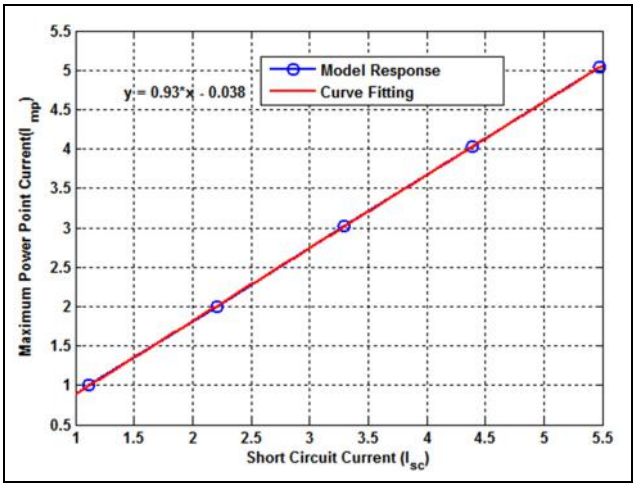

Figure 5. Linear relationship between I_{sc} and I_{mp} under different solar irradiances.

Figure 11 shows the inductor current at the input side of the single stage boost inverter. Further, to study the performance of the inverter during transient conditions, perturbation is given at the grid side. The simulation results of the single stage boost inverter for grid disturbance are presented in Figures 12 and 13. At 10 ms, grid voltage is reduced from 230V RMS to 200V RMS, and again at 16ms, the grid voltage is increased back to 230V RMS. It is evident from the Figure 12 that the capacitor voltages are reduced as well as increased according to the grid voltage disturbance.It ensures the design and operation of the output voltage control algorithm. From the Figure 13, it is observed that the grid voltage gets changed, due to its disturbance whereas, current injected into the grid remains unchanged, since it is not perturbed.

In order to validate the performance of the current control algorithm, disturbance is given at the current injected into the grid and it is decided by the MPPT algorithm. Initially, the PV panel is made to operate at 1000 w/m2 of irradiance (i.e. 5.03 A) and it is decreased to 600 w/m2 (i.e. 3.01 A) at 12ms as shown in Figure 14. The inductor current which occurs due to grid current disturbance is shown in Figure 15. Figures 14 and 15 ensure the design and operation of the current control algorithm. From the Figure 16, it is very clear that the Total Harmonic Distortion(THD) of the boost inverter is very less (i.e. 0.95%) and it satisfies the norms of IEEE 519 standards.

In order to evaluate the performance of the proposed photovoltaic fed single stage boost inverter, a laboratory prototype has been developed. The current control algorithm and the voltage control algorithm are implemented in the SPATRAN 3A DSP board as shown in Figure 17.

Further, the figures from 18 to 21 illustrate the results obtained from the hardware prototype. Figure 18 shows the voltage across the capacitors (i.e. V_{b1} and V_{b2}) along

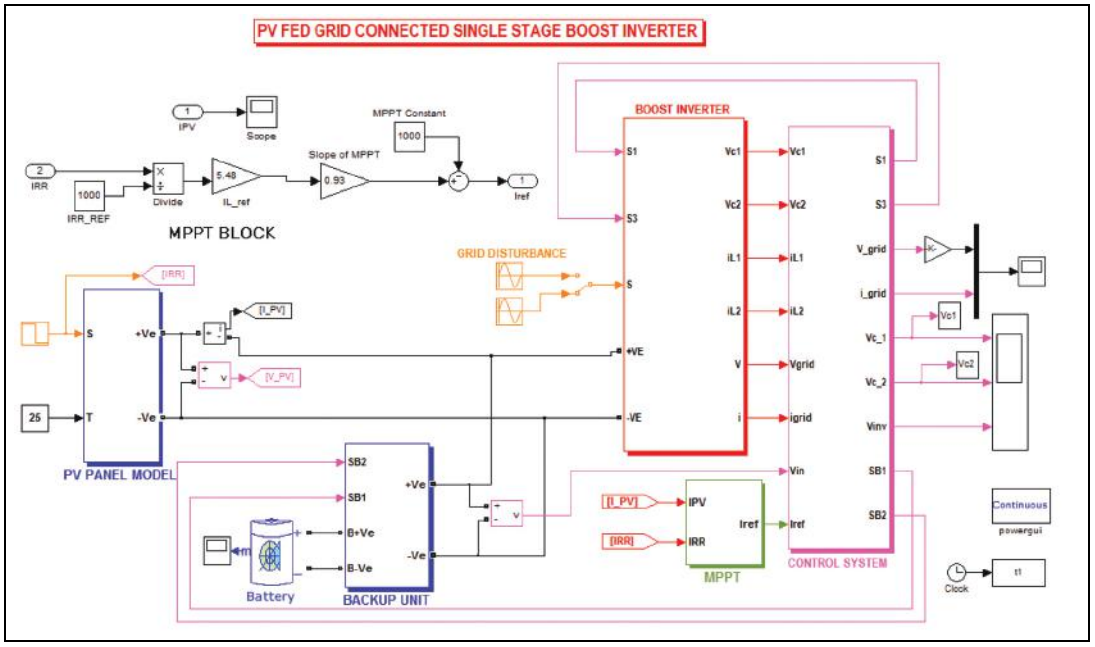

Figure 6. MATLAB/SIMULINK Block Diagram of the Proposed System.

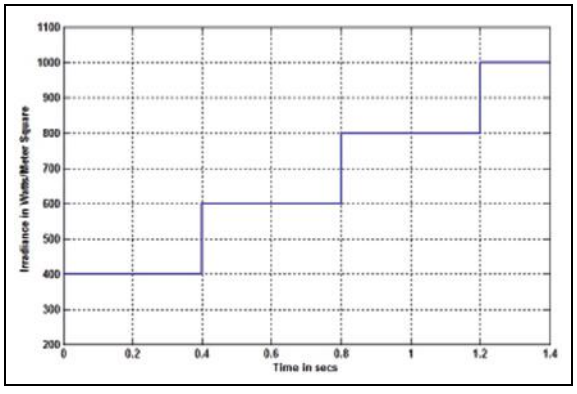

Figure 7. Irradiance pattern given to test MPPT algorithm.

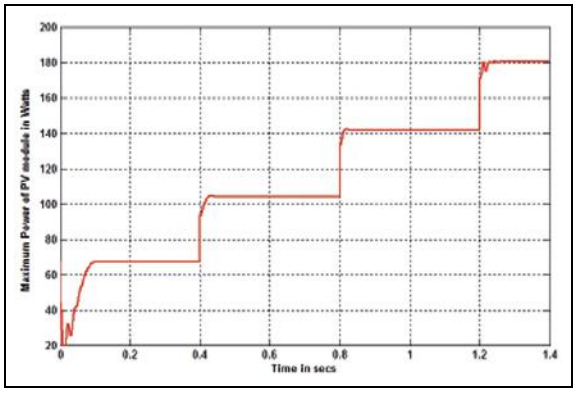

Figure 8. Response of PV Panel for step change in irradiance pattern.

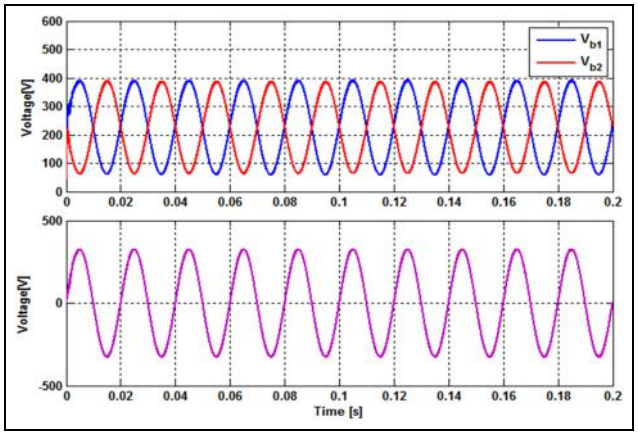

Figure 9. (a) Voltage across capacitors (b) Inverter output voltage.

with the inverter voltage and the current fed into the grid. When compared the Figures 9 and 18, it is seen that both of them match very closely. The experimental results of the THD in the inverter voltage are depicted in Figure 19. The values of THD obtained from the simulation and the hardware results match very closely to each other. The experimental results of the capacitor voltages and the inductor currents are portrayed in Figure 20. When the simulation results obtained from the Figures 6 and 8 are compared with the experimental results obtained from Figure 20, it can be seen clearly that both the results are very closer. The hardware results obtained from the prototype for step change in the grid voltage are illustrated in

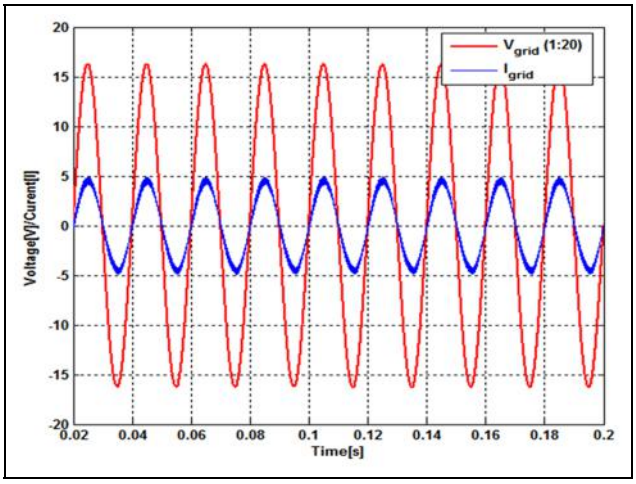

Figure 10. Grid Voltage and Current.

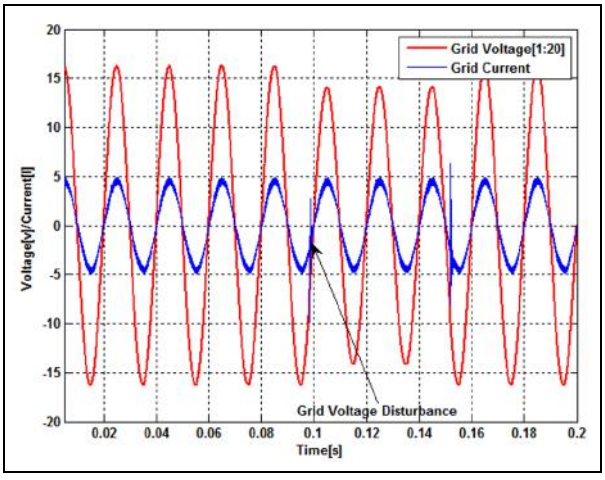

Figure 13. Grid Voltage and Current due to grid voltage disturbance.

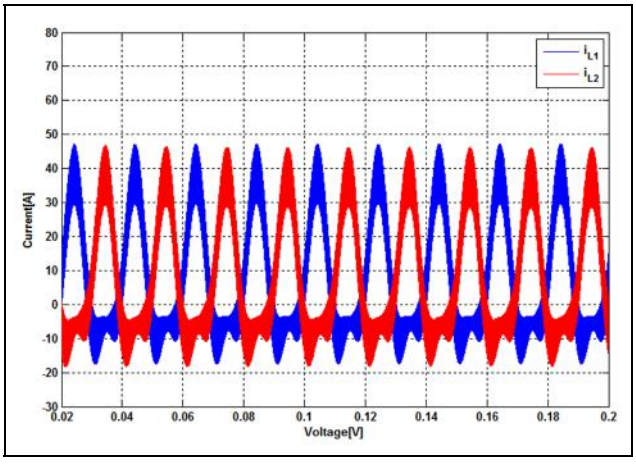

Figure 11. Inductor Current.

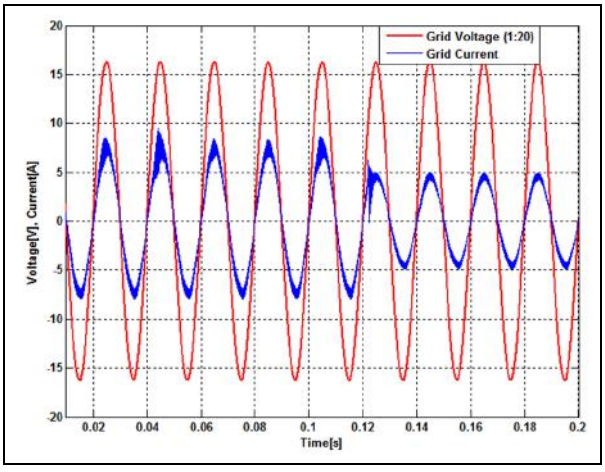

Figure 14. Grid Voltage and Current due to grid current disturbance.

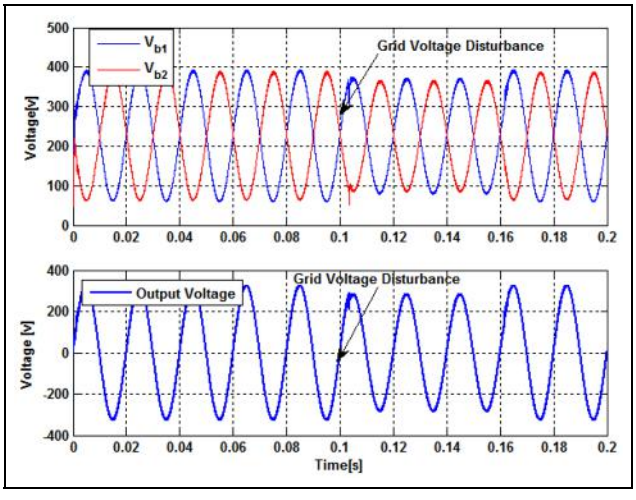

Figure 12. Performace of Inverter due to grid voltage disturbance (a) Capacitor Voltages (b) Inverter Voltage.

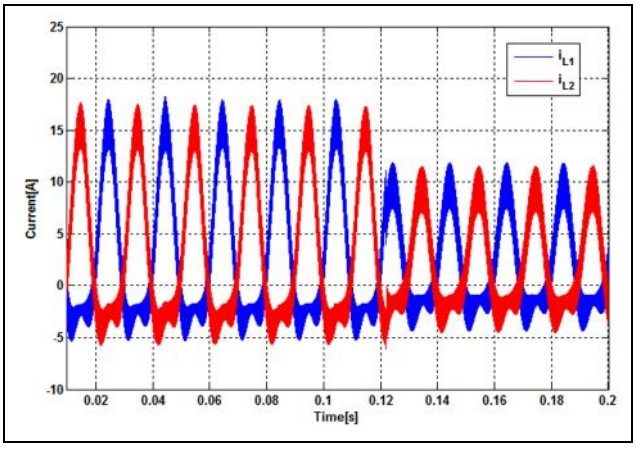

Figure 15. Inductor currents due to current disturbance.

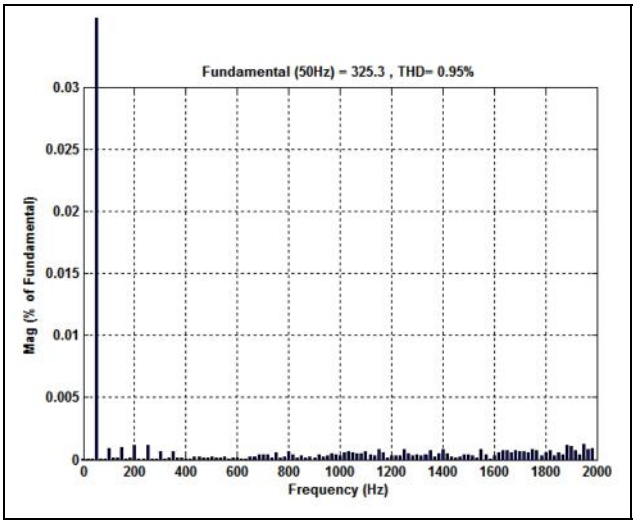

Figure 16. Harmonic Spectrum of Inverter Voltage.

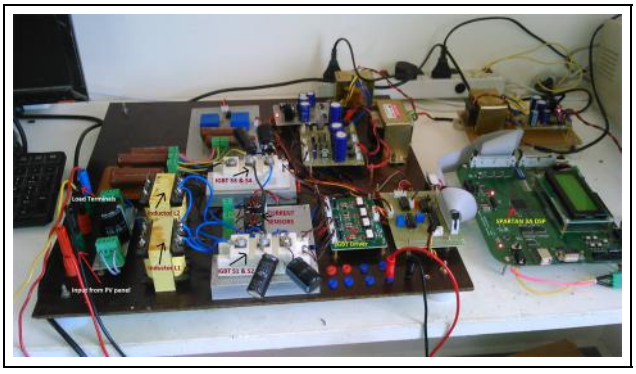

Figure 17. Laboratory Prototype of the proposed PV fed Single stage boost Inverter.

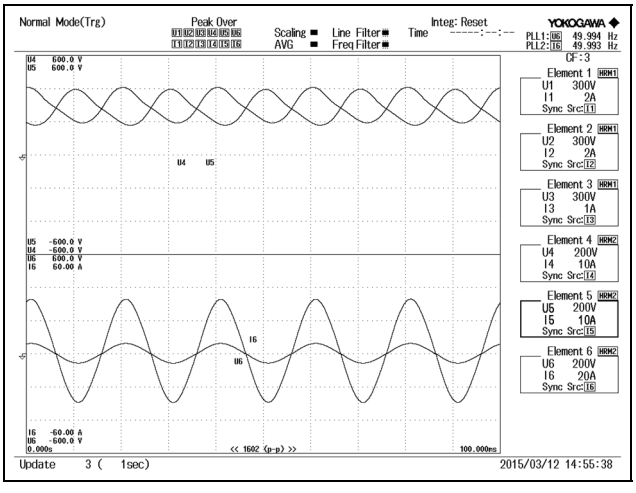

Figure 18. Experimental Results (a) Voltage across capacitors (b) Inverter voltage and current fed into the grid.

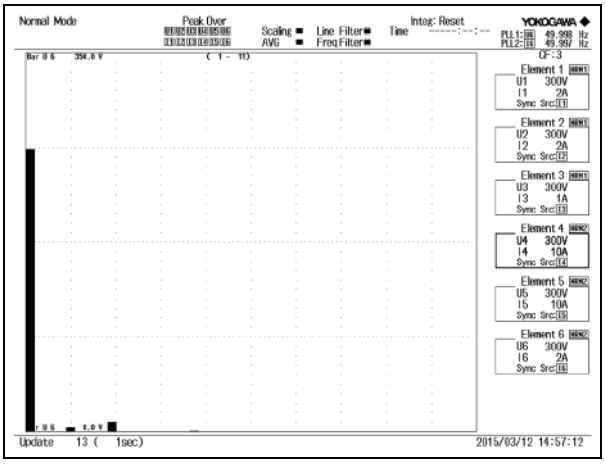

Figure 19. THD waveform obtained experimentally of the inverter voltage.

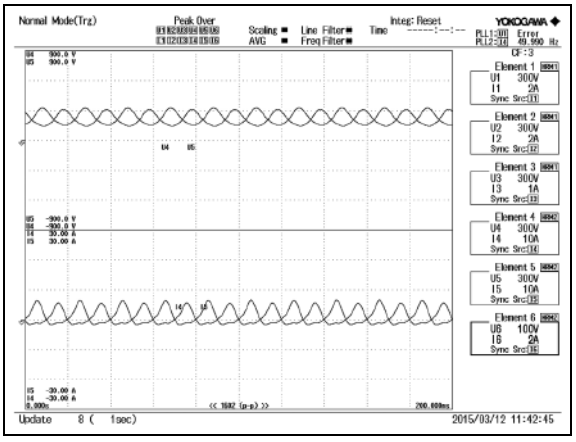

Figure 20. Experimental Results Voltage across capacitors (b) Inductor currents.

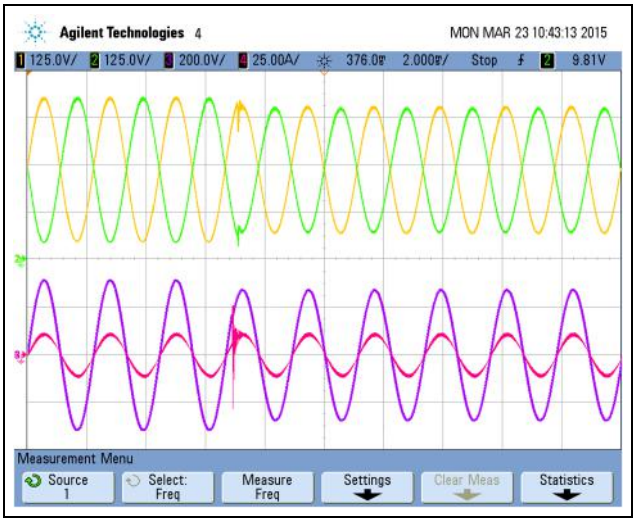

Figure 21. Experimental results for step change in the grid voltage.

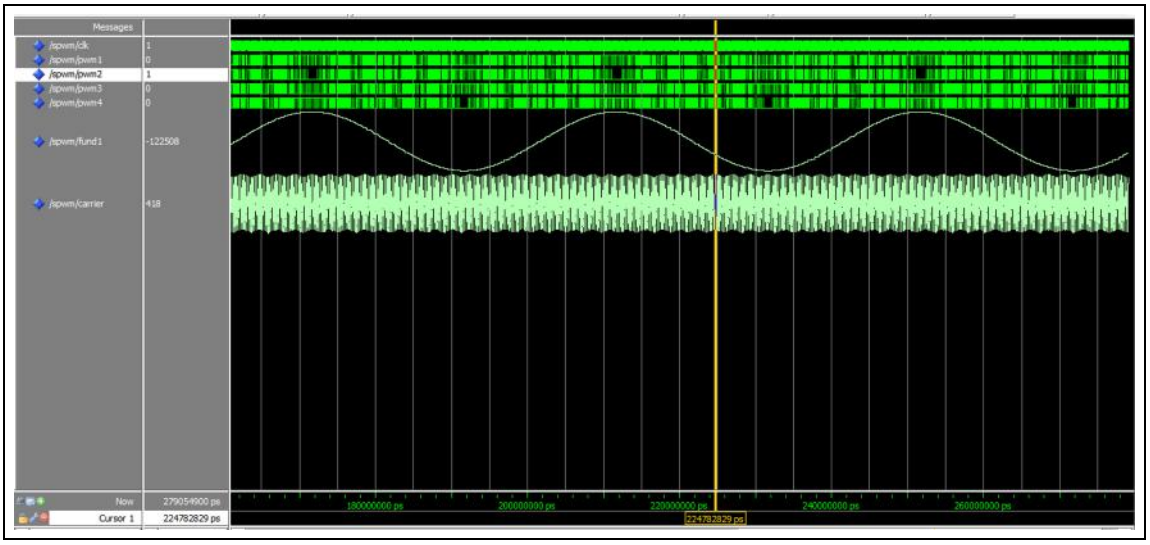

Figure 22. Switching pulses generated through FPGA Simulation.

Table 4. Comparison of THD for Various PV Input Voltages.

PV Voltage	THD (Voltage)		THD (Current)	
	Simulated	Experiment	Simulated	Experiment
38	0.95	1.05	4.88	5.09
36	1.19	1.15	5.32	5.65
34	1.32	1.26	5.76	5.98
32	1.69	1.95	6.14	6.38
31	1.76	2.32	8.04	8.89

Figure 21. When the Grid voltage is suddenly reduced after a few cycles, the capacitor voltage and the inverter voltage consequently get reduced as shown in Figure 21. Figure 22 shows the simulation results of the switching pulses which are obtained from Modelsim tool.The performance of the proposed inverter is described in Table 4 with respect to various solar irradiance levels. It is very evident from the Table that the performance of the proposed inverter is enhanced in terms of Total Harmonic Distortion. THD seems to be little increased for low irradiance levels (i.e. when the output voltage of solar PV is minimum), but still the THD level is below the standard of IEEE 519.

4. Conclusions

In the present work, a single-phase grid-connected single stage boost inverter photovoltaic system topology with a battery backup based energy storage unit has been proposed. The operation characteristics of the proposed PV system are verified through simulation and experimental results. The results are evident that the proposed system provides many advantages, such as single stage power conversion with high efficiency, simple circuitry and low cost. Moreover, this system possesses the capability to operate in grid-connected as well as in stand-alone modes. Further, the proposed inverter is controlled by both the current control algorithm and the voltage control algorithm for maximum power point tracking and for controlling the inverter voltage, respectively in coordination with the grid voltage.

References

1. Tan CW, Green TC and Hernandez CA. An improved maximum power point tracking algorithm with current-mode control for photovoltaic applications. *IEEE International Conference on Power Electronics and Drive Systems* 2005; 1: 489-494.
2. Kjaer SB, Pedersen JK and Blaabjerg F. A review of single-phase grid-connected inverters for photovoltaic modules. *IEEE Transactions on Industry Applications* 2005; 41: 1292-1306.
3. Calais M, Myrzik J, Spooner T, et al. Inverters for single-phase grid connected photovoltaic systems-an overview. Proc. 02 of IEEE 33rd Annual Power Electronics Specialists Conference 2002; 4: 1995-2000.

4. Choi WY and Choi JY. High-efficiency power conditioning system for grid-connected photovoltaic modules. *J Power Electronics* 2011; 4: 561-567.
5. Rezaei MA, Iman-Eini H and Farhangi S. Grid-connected photovoltaic system based on a cascaded H-Bridge inverter. *J Power Electronics* 2012; 4: 578-586.
6. Lee JP, Min BD and Yoo DW. Implementation of a High Efficiency Grid-Tied Multi-Level Photovoltaic Power Conditioning System Using Phase Shifted H-Bridge Modules. *J Power Electronics* 2013; 2: 296-303.
7. Lee JP, Min BD, Kim TJ, et al. Design and control of novel topology for photovoltaic dc/dc converter with high efficiency under wide load ranges. *J Power Electronics* 2009; 2: 300-307.
8. Lee JP, Min BD, Kim TJ, et al. Input-series-output-parallel connected DC/DC converter for a photovoltaic PCS with high efficiency under a wide load range. *J Power Electronics* 2010; 1: 9-13.
9. Lee SH, An TP and Cha H. Mitigation of low frequency ac ripple in single-phase photovoltaic power conditioning systems. *J Power Electronics* 2010; 3: 328-333.
10. Cacciato M, Consoli A, Attanasio R, et al. Soft-switching converter with HF transformer for grid-connected photovoltaic systems. *IEEE Transactions on Industrial Electronics* 2010; 5: 1678-1686.
11. Salameh ZM and Lynch WA. Multi-stage dual priority regulator for photovoltaic systems. IEEE Trans. Energy Conversion 1989; 4: 308-313.
12. Caceres RO and Barbi I. A boost DC-AC converter: Analysis, design, and experimentation. *IEEE Transactions on Power Electronics* 1999; 14: 134-141.
13. Sanchis P, Ursaea A, Gubia E, et al. Boost DC-AC inverter: A new control strategy. *IEEE Transactions on Power Electronics* 2005; 20: 343-353.
14. Oystein Ulleberg, Stand Alone Power systems for the Future: Optimal Design, Operation & Control of Solar-Hydrogen Energy Systems, Ph.D. Dissertation, Norwegian University of Science and Technology 1998, Trondheim.
15. Jang M and Agelidis VG. A minimum power- processing-stage fuel cell energy system based on a boost-inverter with a bidirectional backup battery storage. *IEEE Transactions on Power Electronics* 2011; 26: 1568-1577.
16. Zhao W, Lu DDC and Agelidis VG. Current control of grid-connected boost inverter with zero steady-state error. *IEEE Transactions on Power Electronics* 2011; 26: 2825-2834.
17. Cortes D, Vazquez N and Alvarez-Gallegos J, Dynamical sliding-mode control of the boost inverter. IEEE Transactions on Industrial Electronics 2009; 56: 3467-3476.
18. Jossen A. Fundamentals of battery dynamics. *J Power Sources* 2006; 154: 530-538.
19. Senjyu T, Shirasawa T and Uezato K. A maximum power point tracking control for photovoltaic array without voltage sensor. *Journal of Power Electronics* 2002; 2: 155-166.
20. Abo-Khalil AG, Lee DC, Choi JW, et al. Maximum power point tracking controller connecting PV system to grid. *Journal of Power Electronics* 2006; 6: 226-234.
21. Mehrnami S and Farhangi S. Innovative decision reference based algorithm for photovoltaic maximum power point tracking. *Journal of Power Electronics* 2010; 10: 528-537.
22. Ahmed EM and Shoyama M. Scaling factor design based variable step size incremental resistance maximum power point tracking for PV systems. *J Power Electronics* 2012; 12: 164-171.
23. Ding K, Wang X, Zhai QX, et al. Improved Global Maximum Power Point Tracking Method Based on Voltage Interval for PV Array under Partially Shaded Conditions. *J Power Electronics* 2014; 14: 722-732.
24. Tian Y, Xia B, Xu Z, et al. Modified asymmetrical variable step size incremental conductance maximum power point tracking method for photovoltaic systems. *J Power Electronics* 2014; 14: 156-164.
25. Esram T and Chapman PL. Comparison of photovoltaic array maximum power point tracking techniques. *IEEE Transactions on Energy Conversion* 2007; 22: 439-449.
26. Masoum MAS, Dehbonei H and Fuchs EF. Theoretical and experimental analyses of photovoltaic systems with voltage and current-based maximum power-point tracking. *IEEE Transactions on Energy Conversion* 2002; 17: 514-522.
27. Enslin JH, Wolf MS, Snyman DB, et al. Integrated Photovoltaic Maximum Power Point Tracking Converter. *IEEE Transactions On Industrial Electronics* 1997; 44: 769-773.